J. Fluid Mech. (1973), *vol.* 60, *part* 2, *pp.* 285–303
Printed in Great Britain

Some further studies on the transition to turbulent convection

By RUBY KRISHNAMURTI

The Geophysical Fluid Dynamics Institute and The Department of Oceanography, Florida State University, Tallahassee

(Received 20 July 1972 and in revised form 5 March 1973)

In a horizontal convecting layer of fluid, several distinct transitions occur at certain distinct Rayleigh numbers R, for a given Prandtl number Pr. The regime diagram has been extended to include the Prandtl-number range

$$2{\cdot}5 \times 10^{-2} \leqslant Pr \leqslant 0{\cdot}85 \times 10^{4}.$$

In particular it is found that distinct changes in the slope of the heat-flux curve occur even for $Pr = 2{\cdot}5 \times 10^{-2}$. The flow is steady up to $R = R_t = 2{\cdot}4 \times 10^3$. For $R > R_t$, the period of oscillation is compared with the theoretical values of Busse. For $Pr \leqslant 0{\cdot}71$ decreases as well as increases in the slope of the heat-flux curve are observed.

For R just greater than R_c, the preferred orientation of rolls in various side-wall geometries is investigated. For high Prandtl number, the effect of curvature of the roll axis, forced by curved side walls, upon the second transition at R_{II} is investigated. It is found that curvature, as well as previously discussed effects, leads to a lowering of R_{II}. These results, along with the observed hysteresis, support the view that there are metastable states attainable by finite amplitude instability. Finally the nature of the time-dependent flow at large R and high Prandtl number is investigated in a Hele-Shaw cell. It is shown unequivocally that the observed periodicity at a fixed point is due to hot or cold plumes moving past the point.

1. Introduction

This paper describes an extension of previous studies on the transition to turbulent convection. In particular it includes an investigation of (i) the heat-flux transitions at low Prandtl number, (ii) the preferred orientation of rolls in various side-wall geometries, (iii) the effect of curvature of the roll axis upon the second transition at R_{II} (for high Prandtl number) and (iv) the nature of the time dependence for high Prandtl number.

The Rayleigh number R is defined in the usual manner: $R = (g\alpha/\kappa\nu)\Delta T d^3$, where g is the acceleration of gravity, α is the thermal expansion coefficient, κ is the thermal diffusivity, ν the kinematic viscosity, ΔT the temperature difference between bottom and top of the layer, and d is the layer depth. The Prandtl number Pr is the ratio of ν to κ.

Previous studies (Malkus 1954; Willis & Deardorff 1967*a*, *b*, 1970; Busse 1968; Krishnamurti 1970*a*, *b*; the latter will be referred to hereafter as I and II) have shown that in the horizontal convecting layer a number of discrete transitions occur before the flow becomes fully turbulent. In the order of increasing Rayleigh number R the first is the well-known transition at the critical value R_c from the static conduction state to steady two-dimensional convection. For Prandtl numbers $Pr \geqslant 7$, the second is a transition, at $R_{\mathrm{II}} \simeq 12R_c$, from steady two-dimensional to steady three-dimensional flow. The third occurs at a Rayleigh number R_t dependent upon Pr and is a transition to time-dependent flow. Thus one forms the picture that, as the Rayleigh number is increased, the system approaches turbulence by becoming unstable to more and more kinds of disturbances. Each of these three types of transitions was accompanied by an increase in the slope of the heat-flux curve and hence an increase in the effective conductivity of the layer. Although this seemed most reasonable at $R = R_c$ and Pr large, it was not always clear why each new instability should be associated with an increase in slope. Examples are now found at low Pr for which decreases of slope occur. The regime diagram has been extended so that it includes

$$2{\cdot}5 \times 10^{-2} \leqslant Pr \leqslant 0{\cdot}85 \times 10^{4}.$$

For Prandtl numbers approaching zero, the dimensional heat-flux curve is expected to show no change of slope as R increases through R_c. This is intuitively clear, and it can also be seen from small amplitude nonlinear theories. If the Boussinesq equations are scaled using the depth d for the length scale, d^2/κ for the time scale, κ/d for the scale of velocity u_i and $\Delta T/R$ for the scale of fluctuating temperature θ, one obtains the usual equations with $Pr^{-1}u_j\,\partial u_i/\partial x_j$ and $u_j\partial\theta/\partial x_j$ for the nonlinear advection terms. The small amplitude expansion techniques are applicable where these terms are small compared with the linear terms and hence inapplicable as $Pr \to 0$. By rescaling the equations using d for the length scale, d^2/ν for the time scale, ν/d for the velocity scale, ΔT for the scale of the static temperature and $\Delta T Pr/R$ for the scale of θ, one obtains

$$\begin{aligned}
\nabla^2 u_i + \lambda_i\theta - \partial\pi/\partial x_i &= u_j\,\partial u_i/\partial x_j,\\
\nabla^2\theta + Ru_j\lambda_j &= Pr\,u_j\,\partial\theta/\partial x_j,\\
\partial u_j/\partial x_j = 0, \quad \boldsymbol{\lambda} &= (0, 0, 1),
\end{aligned}$$

where π is a modified pressure. The results of Schlüter, Lortz & Busse (1965) can then be used to show that, for $Pr \to 0$, the dimensional convective heat flux becomes

$$\langle w\theta\rangle = \frac{Pr^2}{R}\left(\frac{R-R_c}{a}\right)\kappa\frac{\Delta T}{d},$$

where a is an integral computed by Schlüter *et al.*; for rolls between rigid boundaries, $a = 0{\cdot}00832$. This result is compared with the experimentally determined heat flux for $Pr = 2{\cdot}5 \times 10^{-2}$.

In a horizontally infinite layer there is no preferred orientation of the rolls. For a laboratory experiment, where the layer is necessarily truncated by side walls, Davis (1967) and Segel (1969) have discussed the question of how shallow

the layer must be to approximate an infinite layer. They have shown that, for a shallow rectangular layer, rolls should line up with their axes parallel to the short side of the container. This orientation minimizes the ratio of the rate of viscous dissipation of kinetic energy to the rate of release of potential energy by the buoyancy force. Expressed in another way, the preferred orientation is one in which the rolls meet most of the side boundaries at right angles. The effect of the side walls penetrates approximately two roll widths inwards from the side walls. Although the theory is for perfectly conducting side walls which would almost never be used in an experiment, certain features controlled by viscous dissipation can still be expected to be observed.

Segel has further discussed wall modes, such as ring-shaped rolls that fit in a circular container (Koschmieder 1966), for which the side walls affect the entire convecting layer. Similar wall-induced flows were observed (Krishnamurti 1967) in a square container, one subcritical roll being seen along each of the four side walls. As the Rayleigh number was slowly increased beyond R_c, more rolls formed along the subcritical roll, so that a square pattern of rolls was formed, with those rolls parallel to one wall meeting the perpendicular ones along the diagonals of the square tank. It was explained that the subcritical rolls were produced by a fringing of the isotherms due entirely to the fact that the horizontal layer was truncated. This fringing implies a horizontal temperature gradient which will always drive a flow. Furthermore, it was found that the square array of rolls was unstable as expected, since the flow was three-dimensional along the diagonals and since this can be, and was in fact, replaced by rolls everywhere parallel to one boundary or everywhere perpendicular to that boundary. This fringing of isotherms due to truncation can be made very small if the side walls have very nearly the same thermal conductivity as the fluid and are either very thick or are surrounded by more fluid of the same conductivity. Indeed it is found that, with such an arrangement, the ring-shaped wall mode is not realized, but instead the rolls tend again to meet most of the walls at right angles.

When the heat flux and Rayleigh number are decreased from a value greater than R_{II}, a hysteresis both in the heat-flux curve and in the flow form is observed (I). The heat flux at a given R is larger than it was when R was increased from lower values, the roll width is larger, and the three-dimensional disturbance persists to Rayleigh numbers as low as $4{\cdot}5R_c$. It was shown in I (figure 8*b*) that if R were changed too rapidly ($R_c^{-1}\,dR/dt = 6 \times 10^{-5}\,\mathrm{s}^{-1}$, where the thermal diffusion time is $d^2/\kappa = 3{\cdot}4 \times 10^3\,\mathrm{s}$) the three-dimensional disturbance could be amplified at $R = 4R_c$. It should be noted, however, that a three-dimensional disturbance with a very distinctive wavelength is already present (visible in figure 8 (*a*) of I, and also very apparent in figure 5 (*a*) of Krishnamurti 1968*b*) because the convection was started as a 'wall mode', i.e. as a square array of rolls. In most laboratory experiments a desired value of R is reached fairly rapidly, usually from below, and rolls are usually curved. If rolls are curved and already contain some three-dimensional regions for R below R_{II} because of initial or boundary conditions (and R is always increased from below) how will the magnitude of R_{II} be affected? It is found that R_{II} can be considerably reduced.

The third transition in order of increasing R, for $Pr \geqslant 6{\cdot}7$, occurs at a Rayleigh

number which will be labelled R_t. It marks a change from a steady three-dimensional to time-dependent flow, and has associated with it a discrete change in the slope of the heat-flux curve. The nature of the time dependence has been discussed by Krishnamurti (in II) and by Willis & Deardorff (1965, 1967*a*, 1970). In II the nature of the time dependence was studied by means of x, t photographs, where x is a horizontal co-ordinate and t is the time, synchronized with temperature measurements. In steady cellular flow, the cell boundaries remain fixed in time; the tracer particles make herring-bone-like patterns as they move towards or away from cell boundaries. At higher Rayleigh numbers, x, t photographs show bright spots corresponding to regions of strong shear moving in the following manner. When the light beam is near the bottom (top) of the layer, a bright spot moves from the cell boundary where there is descent (ascent) of fluid across to the next cell boundary where there is ascent (descent). This process is repeated periodically with time. (See, for example, figures 4 (*f*) or (*h*) in II.) This horizontal movement of the bright spot is found with the light beam near the top or bottom of the layer, but *never* with the light beam at mid-depth. At mid-depth oscillations of brightness with time can be seen, but no horizontal motion is detectable. (Compare figures 4 (*c*) and (*d*) in II.) Of course, as was mentioned in II, oscillations of brightness in time with no horizontal motion were found even near the bottom and top boundaries in cases where the light beam intersected a cell in which the flow was in the line of sight. In all cases, of the several hundred x, t photographs studied, the bright regions were observed to move with the local cellular flow. This behaviour cannot be called depth independent. If the flow in a particular cell, say near the lower boundary, is from left to right (so that the characteristics on the x, t photograph have positive slope), then the bright spots move from left to right repeatedly, always with positive slope, and never oscillating from positive to negative slope. This behaviour is not consistent with oscillating rolls corresponding to a wave travelling along the roll axis as is found for low Prandtl numbers. For high Prandtl numbers, as the bright spots approach a cell boundary periodically the latter may oscillate, but the bright spots should not be eliminated from consideration as has been suggested.

Difficulties in interpretation arising from II might be mentioned. If the bright spots had been due to fall-out of aluminum flakes, there should have been a noticeable difference between observations made immediately after stirring or after several weeks of continued convection. There should have also been a noticeable difference between the cases of $Pr = 10$ or $Pr = 10^4$, since for $Pr = 10^4$ the settling of aluminum flakes requires several months. There were no such differences observed. Of course temperature anomalies were obtained with or without tracers. Moving bright regions as described above are apparent in Rossby's (1966) time-lapse movies, where in plan view bright flashes move horizontally, and in elevation periodic surges of a bright region are seen. The interpretation of bright regions when aluminum flakes are used as tracers requires care. One interpretation is that they are regions of strong shear. Another is that bright regions represent high concentrations of aluminum flakes. In II, care was taken in its use so that the first interpretation was valid. The x, t photographs in II display only one dimension and thus an incomplete picture of

the flow. Another difficulty stems from the fact that the bright regions are diffuse or poorly defined, and can easily be interpreted as patches of high tracer concentration. It became clear that the latter problem would be overcome by choosing a fluid of high thermal expansion coefficient and low thermal diffusivity. Freon 113 or Rheoscopic fluid FW 101 is just such a fluid. The thermal expansion coefficient of freon 113 is about 7 times that of water; the thermal diffusivity is about half that of water. A sealed glass tank $7 \times 12 \times 1{\cdot}5$ in. deep containing a mixture of these two fluids was heated below and cooled above. Distinct growing plumes were easily observable moving with the larger scale flow. However this large-scale flow itself was quite disorderly. It was felt that a more orderly flow that would have an x, t photograph as in II, figure 4(f), showing a simple movement of plumes would be much more instructive than a flow more disorderly than that in II, figure 4(g). In this paper, we show convection in a confined region (a Hele-Shaw cell) heated below, to demonstrate the fact that hot spots or plumes are advected by an orderly larger scale (Bénard cell) flow.

The flow of homogeneous fluid in a Hele-Shaw cell has been discussed by many authors (Hele-Shaw 1898; Lamb 1932, p. 582). Cellular convection in a Hele-Shaw cell has been discussed in a series of papers by Wooding and by Elder, who gives a complete bibliography (Elder 1967).

In II, the periodicity described above was found in x, t photographs at $R \geqslant R_t$. Of course a value of R considerably greater than R_t was used to obtain a strong signal and a clear picture of this periodicity. In this paper, the Hele-Shaw cell is used to demonstrate the nature of a time-periodic flow that develops when one degree of freedom is removed. Again the observations are taken at R much greater than that at which time-periodic flow first develops, in order to obtain a clearer and more interesting picture than at the marginal state. Most of the photographs shown here are at a Rayleigh number around $500R_c$, where $R_c = 3{\cdot}7 \times 10^5$, although occasional plumes could be seen at R as low as $50R_c$, for example. It should become clear from the photographs presented here than an x, t representation similar to those in II would be obtained for the time-dependent Hele-Shaw flow. The Hele-Shaw flow is presented as a clearer demonstration of the type of time dependence found in II for a fully three-dimensional flow at large Pr and $R \geqslant R_t$.

2. Apparatus and procedure

The apparatus and experimental procedure used for part of this study were essentially as described in I and II. After a brief summary of these, modifications will be described. A Plexiglas tank of inside dimensions approximately $20 \times 20 \times 13$ in. deep contains the following layers of materials from the bottom upward. The first layer is a 4 in. thick block of aluminum, at temperature T_1, with an electrical heater attached to its underside. Next is a low conductivity or 'dummy' layer consisting of a $\frac{1}{16}$ in. thick layer of fluid, a $\frac{1}{4}$ in. thick layer of Plexiglas and another $\frac{1}{16}$ in. layer of fluid. Next is a 1 in. thick layer of aluminum, at temperature T_2. Next is the fluid layer, which occupies a region 49 cm by 49 cm and a depth d. Values for d of 0·988, 1·984, 3·007 or 5·000 cm were used. Above

the fluid is a 1 in. thick layer of aluminum, at temperature T_3. Above this is another dummy layer of Plexiglas, then above this a 4 in. thick block of aluminum, at temperature T_4. This block has channels cut in its upper side for the circulation of the cooling fluid. Details will be found in I. Because of the high conductivity of aluminum compared with that of the convecting fluid, vertical temperature gradients in the aluminum blocks are too small to measure. Hence the heat transported by the convecting fluid is determined by measuring the vertical temperature gradient across the dummy layer. Because it has a relatively low conductivity, $T_1 - T_2$ is large enough to be easily measured. Then, knowing the depth d_p and the molecular conductivity k_p of the dummy layer from a separate measurement, the heat transported upwards is determined as

$$H = \frac{k_p}{d_p}\left[\frac{T_1 - T_2}{2} + \frac{T_3 - T_4}{2}\right],$$

where we have taken the two dummy layers as identical and averaged the flux through the two. In a steady-state experiment this is also the heat transported upwards by the convecting fluid, neglecting lateral losses, which have been estimated in I to be less than 5 % of the vertical transport. To determine Rayleigh numbers, only $T_2 - T_3$ and d were measured. The tabulated values of α, κ and ν shown in table 1 were used.

All experiments reported here were performed as externally steady, fixed heat flux experiments. The power input was set at some desired value, then the temperature of the cooling fluid was adjusted until all four aluminum blocks reached steady temperatures. This was always possible to attain even when the convective flow itself was time dependent. Mean temperatures were held sufficiently constant (to within $\pm \frac{1}{4}$ °C or even $\pm 0{\cdot}1$ °C depending upon the fluid) so that data reduction would not involve a calculation of the variation of material properties with temperature. In view of the hysteresis found in I and II, care was always taken to change H in one direction only. For example, H was increased by a few per cent at a time and an external steady state was established before making observations. Then H was increased again. H was never allowed to decrease until the desired upper value for a series of experiments was reached.

The heat-flux transitions in air were determined in this way. Time dependence was determined from temperature traces from a thermocouple junction 0·5 mm in diameter that protruded from the upper boundary of the fluid layer 1·6 mm into the fluid. The most sensitive range of the microvolt amplifier is 0·3 μV full scale. Thus ideally, when care is taken with shielding and prevention of stray e.m.f.'s, a temperature difference of 5×10^{-4} °C can be detected using copper–constantan thermocouples. The imposed temperature difference is of the order of one degree. The response time of such an amplifier is slow (of the order of 1 s). However, time dependencies in the fluid were much slower; no time dependencies were ever encountered that approached the limit of resolution in time.

The heat-flux transitions in mercury were obtained in a similar manner. However, in this case a new tank of 1 in. thick Plexiglas with 20 in. square plates of copper instead of aluminum was used. The difference in thermal properties is shown in table 1. It was found that painting the copper with rust-resistant paint

Fluid	α $(°C)^{-1}$	k (cal cm^{-1} s^{-1} $°C^{-1}$)	κ ($cm^2 s^{-1}$)	ν ($cm^2 s^{-1}$)	Pr	d (cm)
Mercury	$1{\cdot}819 \times 10^{-4}$	$1{\cdot}91 \times 10^{-2}$	$4{\cdot}2 \times 10^{-2}$	$1{\cdot}16 \times 10^{-3}$	$2{\cdot}5 \times 10^{-2}$	1·0
Air	$3{\cdot}37 \times 10^{-3}$	$6{\cdot}0 \times 10^{-5}$	0·26	0·18	0·71	3·0, 5·0
Water	$2{\cdot}13 \times 10^{-4}$	$1{\cdot}41 \times 10^{-3}$	$1{\cdot}43 \times 10^{-3}$	$1{\cdot}0 \times 10^{-2}$	6·7	7·6
Freon 113	$1{\cdot}390 \times 10^{-3}$	$2{\cdot}379 \times 10^{-4}$	$0{\cdot}682 \times 10^{-3}$	$4{\cdot}76 \times 10^{-3}$†	7	7·6
Silicone oil	$0{\cdot}96 \times 10^{-3}$	$3{\cdot}8 \times 10^{-4}$	$1{\cdot}16 \times 10^{-3}$	1·0	$0{\cdot}86 \times 10^{3}$	1·0, 2·0
Boundary						
Aluminum	—	0·50	0·87	—	—	—
Copper	—	0·92	1·0	—	—	—
Glass	—	$2{\cdot}5 \times 10^{-3}$	$5{\cdot}0 \times 10^{-3}$	—	—	—

† This data is taken from Benning & Markwood (1939). The remainder of the table is data taken from the *Handbook of Chemistry and Physics*, 39th edn.

TABLE 1

was sufficient to prevent amalgamation with mercury. The tank was built with four threaded, vertical, teflon rods attached to the base of the tank in each corner. Each plate was carefully lowered into a layer of mercury so that air bubbles would not be trapped, then bolted down to prevent floating with four teflon nuts which were precisely machined to act as spacers. The first plate was levelled to within $\pm$ 0·0003 in. of 12 in. All plates were machined to be flat to within $\pm$ 0·0005 in. The most convenient dummy layer was a $\frac{1}{8}$ in. thick sheet of glass. A d.c. power supply produced constant ohmic heating in a 20 in. squared fine mesh of resistance material which was electrically isolated from both the copper plate and fluid. Time dependence was determined again as described above.

To study the preferred orientation of rolls in various geometries, silicon oil of Prandtl number $0{\cdot}86 \times 10^3$ was used with aluminum boundaries above and below. The thermal conductivity of the fluid is $3{\cdot}8 \times 10^{-4}$ cal $cm^{-1} s^{-1} °C^{-1}$, that of the Plexiglas inserts is approximately 5×10^{-4} cal $cm^{-1} s^{-1} °C^{-1}$. The following Plexiglas spacers of depth d were inserted into the fluid layer: (i) a long rectangular rod, $d = 0{\cdot}988$ cm, that divided the fluid layer such that one region was 49 cm by 18 cm; (ii) two rectangular rods, $d = 0{\cdot}988$ cm, that simultaneously divided the fluid layer such that one region was a long rectangle parallel to the line of sight and another was a long rectangle perpendicular to the line of sight; (iii) a circular ring of Plexiglas, $d = 1{\cdot}00$ cm, inside diameter $D = 19{\cdot}1$ cm, outside diameter 20·2 cm and aspect ratio $D/d = 19{\cdot}1$; (iv) a circular ring of Plexiglas, $d = 1{\cdot}00$ cm, inside diameter 6·3 cm, outside diameter 7·6 cm and $D/d = 6{\cdot}3$; (v) the circular ring of (iv) inside the ring of (iii) producing an annular region of depth $d = 1{\cdot}00$ cm and gap width 5·71 cm; (vi) a circular ring of Plexiglas, $d = 2{\cdot}00$ cm, inside diameter 44 cm and $D/d = 22$.

The 'plan forms' of convection for these various geometries were obtained by photographing aluminum flake tracers suspended in the fluid with a mechanically driven camera viewing the flow from the side. As a light beam scans the layer, the camera is moved in such a way that the light from different parts of the layer forms images on different parts of the film. This has been described elsewhere

(Krishnamurti 1968*a*). With Plexiglas rings in the fluid layer, a glare results from reflexion of light into the camera at the four points where the light beam strikes the ring at a 45° angle. Also, the smaller ring was slightly frosted so that the glare is minimized, but it casts an apparent shadow since in this method of photography the camera must look through the ring when the illumination is behind it.

To demonstrate the nature of the time dependence found in II, the following apparatus and procedure were used. A Hele-Shaw cell was constructed using two sheets of $28 \times 4 \times \frac{1}{4}$ in. thick Plexiglas. The two sheets were separated by $\frac{1}{4}$ in. wide strips of $\frac{1}{16}$ in. thick Plexiglas and sealed together in such a way that the liquid occupied a region approximately $27{\cdot}5 \times \frac{1}{16}$ in. and 3 in. in depth. (The remaining depth of 0·5 in. was occupied by air to allow for expansion of the liquid.) We chose co-ordinates such that x varies from 0 to 27·5 in., y from 0 to $\frac{1}{16}$ in., and z from 0 to 3 in. in the vertical direction. The liquid was heated steadily in time and uniformly in the x direction by means of an electrical heater. This consisted of a 28 in. long piece of resistance wire, of diameter 0·05 mm and total resistance 866 Ω, encased in thin polystyrene medical tubing of $\frac{1}{16}$ in. outside diameter. This tubing containing the wire was laid inside the Hele-Shaw cell along the bottom of the liquid layer. The power input could be varied, but for the photographs shown, it was 1·84 W. Cooling at the top was accomplished in some cases by circulating cold water through a metal tube stretched across the top of the convecting fluid. However, this cooling tube has been omitted for the photographs shown here. The convecting fluids used were silicone oil with aluminum flakes, water with Rheoscopic fluid AQW 010 as tracer, and freon 113 with Rheoscopic fluid FW 005 as tracer. The latter produced the most striking photographs as explained below. Sequences of photographs were taken showing the attainment of a statistically steady state as well as sequences showing the nature of the time dependence. A 16 mm movie was also produced.

3. Experimental results

Heat-flux transitions for low Prandtl number

The heat-flux data are shown in figures 1, 2 (*a*) and 2 (*b*), where the heat flux has been non-dimensionalized so that it is the product of the Nusselt and Rayleigh numbers. Although the changes in slope are smaller than with large Pr, distinct changes of slope are still detectable. Straight-line segments were drawn because the scatter in the data is reasonably small, and because there is a definite change in the temperature trace of the internal thermocouple trace from steady to time dependent at the Rayleigh number labelled R_t. This is analogous to the change to time dependence coincident with a change in slope such as that shown in figure 2 of II (where the change of slope is larger). For mercury, hysteresis was found near R_c. The dots, triangles and squares in figure 1 represent three different sequences each with R increased from below. The crosses represent one sequence with R decreased from above, following the increase in R as shown by the dots. The flow was found to be steady up to $R_t = 2{\cdot}4 \times 10^3$. The time-dependent flow is shown by encircled data points. There is an increase in slope at R_t. There is a third transition at $R = 3{\cdot}4 \times 10^3$, above which the slope decreases. For air, the flow

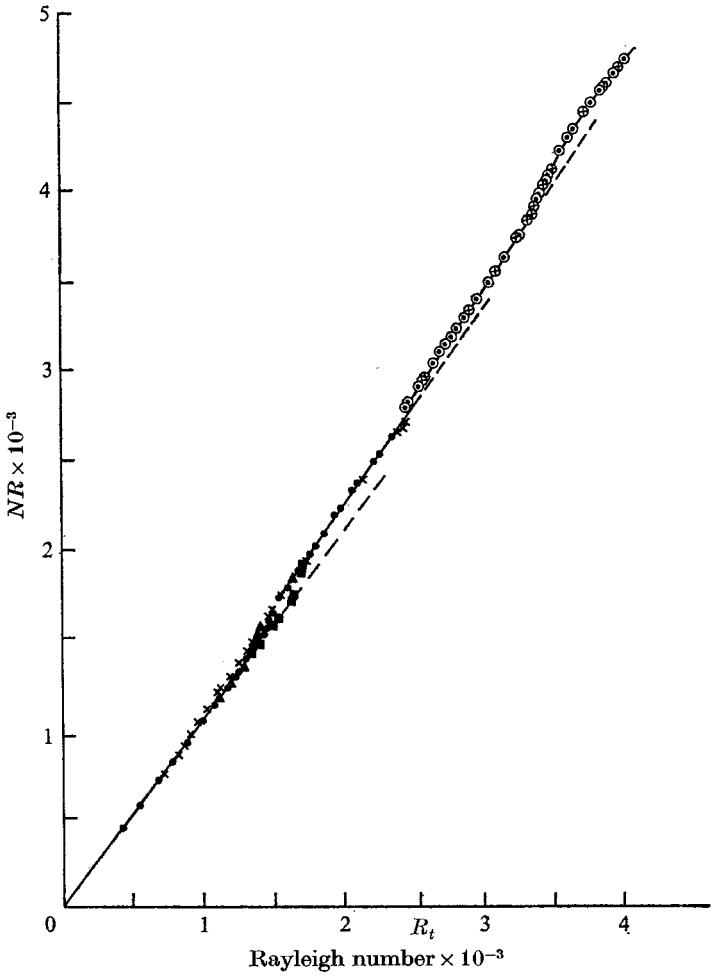

FIGURE 1. Heat flux, non-dimensionalized to equal the product of the Nusselt number N and Rayleigh number R, plotted against R for mercury (Prandtl number = $2{\cdot}5 \times 10^{-2}$). Experimental results: ■, run 1, R increased; ▲, run 2, R increased; ●, run 3, R increased; ×, run 3, R decreased; encircled data points represent time-dependent flow.

was steady up to $R_t = 5{\cdot}6 \times 10^3$, in complete agreement with the earlier results of Willis & Deardorff. There is an increase in slope at $R = R_t$. However, for $R \simeq 1{\cdot}1 \times 10^4$ the heat-flux curve shows a decreased slope for increased R. The slope decreases again at around $1{\cdot}7 \times 10^4$. Some of this data is summarized in table 2 along with results of some previous studies. The quantity dH/dR is interpreted as an effective conductivity of κ_{eff} for the convecting layer.

The response time of the convecting air layer was found to be unusually long compared with the response times of other fluids. When the experimenter increases H by ΔH, the fluid adjusts R by ΔR. By this procedure, it was found that the data point moved to a final steady (H, R) point with R larger than was expected from studies with other fluids (i.e. leading to smaller slope), and moved more slowly than was expected from studies with other fluids. The thermal

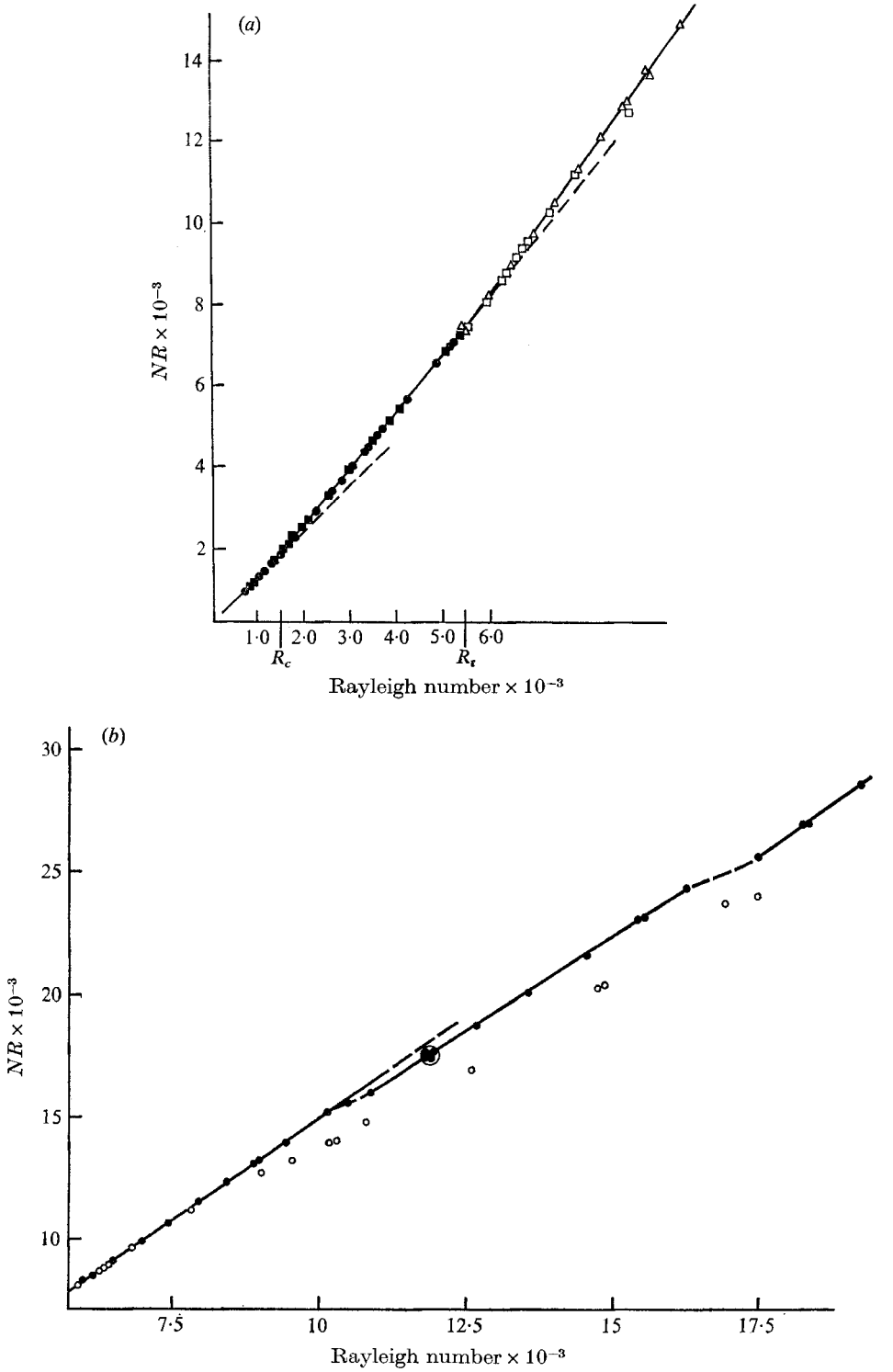

FIGURE 2. Heat flux. NR *vs.* Rayleigh number R for air (Pr = 0·71). (*a*) First two transitions. ●, d = 3·0 cm, steady internal temperatures; △, d = 3·0 cm, time-dependent internal temperatures; ■, d = 5·0 cm, steady internal temperatures; □, d = 5·0 cm, time-dependent internal temperatures. (*b*) Decreases of slope at $R = 6R_c$ and $R = 10R_c$. The cluster of data points at $R = 12 \times 10^3$ shows the amount of drift that occurs in a period of several days. ●, d = 3·0 cm; ○, d = 5·0 cm.

Experimentally determined slopes

Pr	dH/dR for $R_c \leqslant R \leqslant R_{II}$	dH/dR for $R_{II} \leqslant R \leqslant R_t$	dH/dR for $R > R_t$
$2{\cdot}5 \times 10^{-2}$	1·30	—	1·6
0·71	1·37	—	1·6
$0{\cdot}67 \times 10^{1}$	2·72, 2·77	4·66	4·8
$1{\cdot}0 \times 10^{2}$	3·0	4·3	5·6
$0{\cdot}86 \times 10^{3}$	3·1	4·1	5·6
$0{\cdot}85 \times 10^{4}$	3·4	4·2	5·6

Theoretically determined slopes

	Initial slope dH/dR (SLB)†	Average slope dH/dR for $R_c \leqslant R \leqslant 1{\cdot}0 \times 10^4$
$Pr \to 0$	$1 + 1{\cdot}20 \times 10^2\, Pr^2$	—
$Pr = 2{\cdot}5 \times 10^{-2}$	1·08	—
$Pr = 6{\cdot}7$	2·43	2·99 (SV)†
$Pr \to \infty$	2·43	2·95 (B)†

† SLB refers to Schlüter, Lortz & Busse (1965), SV refers to Schneck & Veronis (1967) and B refers to Busse (1968).

TABLE 2

diffusion time $\tau_t = d^2/\kappa$ was 35 s and the viscous diffusion time $\tau_v = d^2/\nu$ was 49 s for one set of experiments with air. For higher Prandtl number fluids, a steady state was reached at least in a time τ_t after external conditions had been changed, but in the case of air more than $50\tau_t$, or about 30 min., was required. Thus, in the case of air, the heat-flux curves are quite different from the quasi-steady curves of Willis & Deardorff. The final state (H, R) remained unchanged for at least several days, to within the scatter (exaggerated by the size of the dots), shown by the cluster of data points around $R = 1{\cdot}2 \times 10^4$ (figure 2*b*). The experiment was repeated several times (once at a different depth) to obtain the entire heat-flux curve, and was found to be completely reproducible.

The period of the time dependence is plotted against the Rayleigh number in figure 3. The period has been made dimensionless by using the viscous time scale d^2/ν. For air, with $Pr = 0{\cdot}71$, it makes little difference whether one uses d^2/κ or d^2/ν. For mercury, however, $d^2/\kappa = 24$ s and $d^2/\nu = 8{\cdot}6 \times 10^2$ s for these experiments ($d = 1{\cdot}0$ cm). The observed periods were of order 10^3–10^2 s. Thus, had the periods been scaled by d^2/κ as with all the other fluids in II, these periods would be decades apart from the others in figure 8 of II. The time dependence first set in with a period of $1{\cdot}14 \times 10^3$ s then increased rapidly with R. Since temperature traces became quite irregular even at R just exceeding R_t, spectral analyses were performed. The multiple peaks of the spectra were read off and plotted in figure 3. Using Busse's (1972) result as stated in his equation (5.2) that the period τ of oscillation measured in units of d^2/κ is related to the wavenumber b by

$$\tau = \frac{2}{3^{\frac{1}{2}} b} \left(\frac{R - R_c}{R_c} \right)^{-\frac{1}{2}}$$

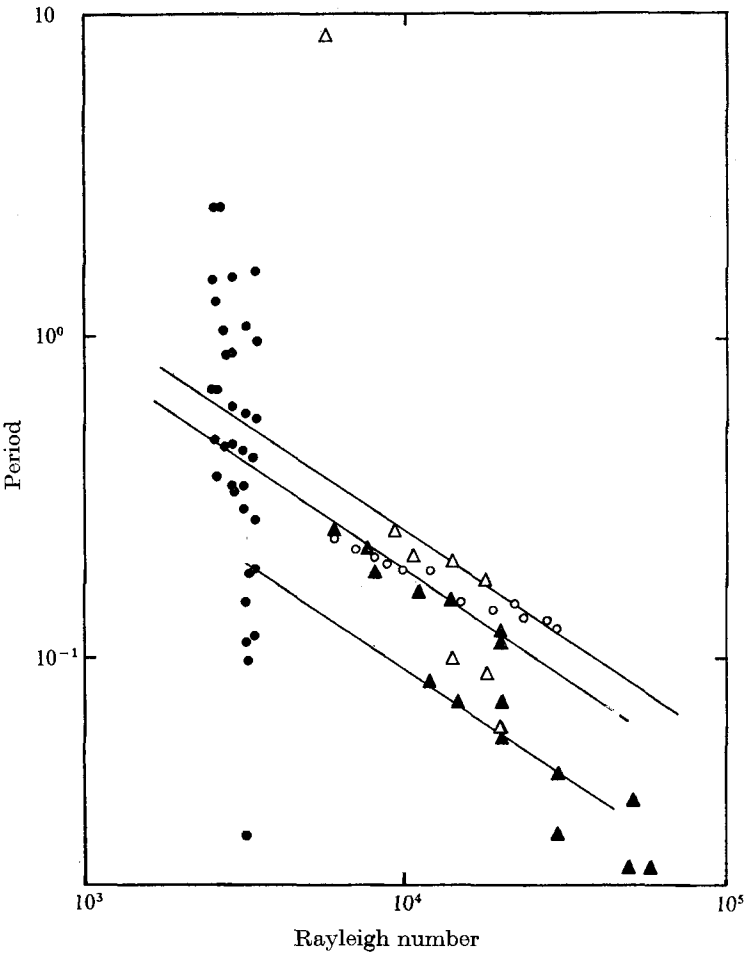

FIGURE 3. The period of oscillation, non-dimensionalized using the viscous diffusion time d^2/ν, plotted against the Rayleigh number. ●, mercury, d = 1·0 cm. Air: ▲, d = 5·0 cm; △, d = 3· cm; ○, Willis & Deardorff (1967*a*), d = 2·5 cm.

the observed periods at $R = R_t$ would correspond to a wavelength of about 200 cm. The convection tank was only 49 cm by 49 cm. It may also be noted that Busse's condition for this instability (his equation (5.1)) gives

$$(R - R_c)/R_c \geqslant 1{\cdot}94 \times 10^{-4}$$

for mercury. Possible reasons for this discrepancy are discussed below. The data are summarized in the regime diagram, figure 4, where the stars indicate observed changes of slope. Above curve III the flow is time dependent. Curve IV marks the next higher change of slope at which higher frequencies were observed. For mercury this change of slope is seen from figure 1 to occur at $R = (3{\cdot}3 \pm 0{\cdot}1) \times 10^3$ while it is seen from figure 3 that higher frequencies appear for $R \geqslant (3{\cdot}15 \pm 0{\cdot}05) \times 10^3$.

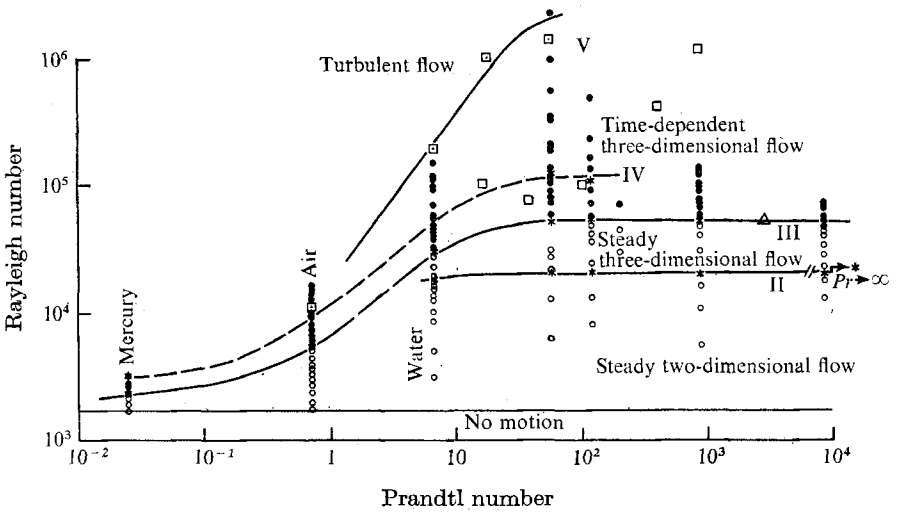

FIGURE 4. Regime diagram. ○, steady flows; ●, time-dependent flows; ★, transition points with observed change in slope; □, Rossby's observations of time-dependent flow; ⊡, Willis & Deardorff's (1967*a*) observations for turbulent flow; △, Silveston's point of transition for time-dependent flow (see text).

Preferred orientation of rolls

These studies can be summarized by stating that rolls prefer to meet most of the lateral boundaries at right angles. For the 49 cm by 18 cm region, the orientation of rolls with axes perpendicular to the long wall is demonstrated in figure 5 (*a*) (plate 1). At least two rolls along each of the shorter walls were found to have modes at right angles to the short wall. Some of this is visible at the extreme left of figure 5 (*a*). In each of the circular regions studied, again rolls met most of the ring boundaries at right angles as shown for example in figure 5 (*c*). Finally, the same preference is shown for the annular region between two rings in figure 5 (*b*). Ring-shaped rolls were not found in any of the rings. In a similar geometry, Chen & Whitehead (1968) found convection patterns similar to figure 5 (*c*) even though they had artificially induced straight rolls by using their light-grid method. This should probably not be ascribed to a fault in the cooling system (Segel 1969), but to a preferred orientation. In another context circular rolls were induced using the light-grid method within a circular boundary which lay in a larger square tank. It was found that the induced ring rolls could not be maintained unless the entire layer were rotating. Without rotation, a mode of convection perpendicular to the circular side wall formed, starting at the outermost ring roll.

Effect of curvature on R_{II}

With the systematic curving of the rolls, forced by the circular boundaries, $D/d = 22$ (figure 5*c*), the heat flux was increased in small steps with long steady periods between each step. The first trace of disturbance is seen at $R = 1{\cdot}3 \times 10^4$ and is well established at $R = 1{\cdot}7 \times 10^4$ (figures 5*d*, *e*). Starting with straight rolls in a square container and increasing R from below, the same form of

disturbance was not well established until $R = 2{\cdot}2 \times 10^4$. For the smallest ring, $D/d = 6{\cdot}3$, the flow appeared three-dimensional from the lowest Rayleigh number observed ($R \simeq 3 \times 10^3$). In figures 5 (*c*) and (*d*), more strongly curved rolls near the wall, where they can be defined as rolls, are not appreciably wider than the rolls in the interior of the ring. The difference in width is not sufficient to explain the lower value of R_{II}. The point is that the disturbance grows throughout the layer.

In summary, there is a definite hysteresis in both the heat flux and the flow pattern when R is decreased from above R_{II}; when R_{II} is approached from below, the two-dimensional flow state appears to be metastable and probably a variety of disturbances including curvature of the roll axis or other local imperfections can lead to the growth of the cross disturbance everywhere and hence to three-dimensional flow for R below $2{\cdot}2 \times 10^4$. The point of establishing the presence of hysteresis and non-uniqueness (dependence upon the initial state or presence of the right fluctuations to excite an early transition) is to show that the transition near R_{II} is a finite amplitude instability. Further the non-uniqueness points to the non-existence of a selection criterion.

Nature of the time dependence at high Prandtl number

Figure 6 (plate 2) is a sequence of photographs showing how the final state in Hele-Shaw convection (frame 12) is attained. After thorough stirring of the fluid, the heater was turned on. Frame 1, taken a few seconds later, shows many thermals, or plumes, which are seen to grow taller in frames 2 and 3. It must be stressed that bright regions do not mean a high concentration of tracer particles; dark regions do not mean a dearth of particles. Although such changes in concentration of tracer particles can occur in general, owing to settling under gravity, this has not occurred in the few seconds between stirring and the photographing of frame 1. The bright regions are those regions in which the shear has aligned the tracer particles such that they strongly reflect the light into the camera. The same region viewed from different angles will not be as bright. Viewed by transmitted light, very little is visible and it is clear that there is *no* noticeable concentration of particles anywhere. For these photographs two lamps were used, one on the left and one on the right of the camera with the light beam making an angle of about 45° with the line of sight. The dark line along the centre of each plume is a line of symmetry along which the shear $\partial w/\partial x$ vanishes. Although gradients in the y direction are larger, these lines of symmetry are still visible presumably because the layer is so thin in the y direction compared with the optical depth. Obviously plumes cannot remain plumes, self-similar or otherwise, when the depth of the fluid is finite. The manner in which they finally are replaced by Bénard-like convection is interesting. Tall skinny plumes tilt and sway with height. If a gap forms between them, a new plume starts to grow from the heated bottom. This new plume gets swept into one or the other of the neighbouring old plumes. The old plume which sweeps up the new one appears to gain strength for it then continues to sweep up every new thermal formed in its vicinity and finally becomes a centre of rising motion. Many such centres form

as may be seen in frame 10, but even some of these are swept up by stronger neighbours and the final state is as in frame 11 or 12. There is in this final state a larger scale of motion which represents the Bénard-like cell and has a horizontal scale comparable with the depth of the layer. For example, in frame 11, there are centres of descending motion at about $5\frac{3}{4}$ in., $11\frac{3}{4}$ in. and at $19\frac{1}{4}$ in. There are centres of ascent at around 9 in., 15·5 in. and 20·2 in. The Rayleigh number is approximately 2×10^8; the critical Rayleigh number is computed to be $3{\cdot}7 \times 10^5$. When R is kept small, either by using low heating rates or a more viscous fluid, this large-scale motion is the only one observed. The flow is then just like that described by Elder (1967) in his figure 8 (*g*) (plate 1). (Elder's Rayleigh number A differs from ours by a factor $(\delta/d)^2$, where δ is the half-width between plates. In terms of A, the critical value A_c is predicted to be $4\pi^2$ and the observed one to be $A_c = 40$.) However, at higher Rayleigh numbers, there is, in addition, a smaller scale motion, namely, the growing plumes, which are better seen close-up (figures 7 (*a*) and (*b*), plates 3 and 4). In figure 7 (*a*) the arrow in frame 1 points at a growing plume which we follow in successive frames. The photographs were taken at 3 s intervals. The plume is seen to grow larger and move to the right. In figure 7 (*a*), frame 3, another plume, indicated by the smaller arrow, is seen forming near the bottom of the descending fluid. The pair of plumes is followed (continued in figure 7 (*b*)) as they grow and move toward the centre of the rising motion. Similarly, one can pick any plume to the right of the centre of rising motion (to the right of the 14 in. mark) and see it grow and move to the left. Thus one forms the following picture of the flow. Hot spots or plumes form along the bottom near the base of the large-scale descent. They travel in the direction of the large-scale flow, growing larger in volume as they move. The fluid out of which they grow can actually be seen to come up through the base of the plume from the region of the warm boundary. They reach the rising region first from the left then from the right, alternating in this way. The rising region waves slightly from left to right as the plumes approach.

Relatively cold spots can be seen forming near the top of the rising column. These also grow and move with the larger scale flow, so that they are somewhat amplified by the time they reach the region of descent (figures 7(*a*), (*b*)). However, they are quite small compared with the hot plumes. When the tube with cooling fluid is used as the top boundary, these cold plumes also amplify greatly and look exactly like a mirror image of the rising region (shifted of course to be centred around the sinking regions). It is not yet known if there is a phase relationship between the hot and cold plumes. However, it is certain that the time-periodic behaviour of convection at high Prandtl number is this periodicity in the Eulerian sense; hot or cold plumes are periodically swept past a fixed point in the fluid. Using the same fluid in a display tank $30 \times 17 \times 3{\cdot}75$ cm in depth, plumes can be seen forming, growing and coalescing just as in the Hele-Shaw cell. Of course, there is much more disorder with this additional degree of freedom and, for example, centres of rising motion do not remain for as great a length of time as in the Hele-Shaw cell.

When other fluids, such as water, are used, similar behaviour is obtained. Small hot spots or plumes are formed occasionally near the bottom and are

advected by the larger scale flow, growing taller as they move. However, use of the fluid FW 005 or freon 113 produces very distinct, sharp thermals. Those formed in water are diffuse by comparison. This is presumably because freon 113 has a much larger thermal expansion coefficient than water and smaller thermal diffusivity, leading of course to increased Rayleigh number. No attempt was made here to define the lowest Rayleigh number at which plumes grow. However, for high Prandtl number (medicinal paraffin) Elder reports no growing plumes at $A = 1{\cdot}10 \times 10^4 = 2{\cdot}7 \times 10^2 A_c$. With water, growing plumes are observed occasionally at $R = 10^7 = 27R_c$.

When the heating rate is lowered plumes are formed less frequently and they move more slowly from the sinking boundary to the rising boundary. The larger the heating rate, the larger the number of plumes visible at any instant. For example, at $R = 10^7$, one or two plumes are seen per cell. At $R = 10^8$, five or six plumes are seen per cell as in figure 7. At very large heating rates plumes coalesce with one another, even before they reach the rising centre. Transition to disorder does indeed seem to result from an increase in the frequency of oscillations (in the Eulerian sense). The flow in the Hele-Shaw cell with steady heating looks statistically similar to that in frame 12 of figure 6, when viewed almost at any time, with one exception. Occasionally, a hot spot forms precisely under the centre of the cold descending flow. Then it is swept neither to the left nor to the right. If it does not move, it grows quite large while remaining right under the descending flow. If this occurs thermals formed later move into it, making it a new centre for rising motions and disrupting the periodicity of the large-scale flow. Another day or two must pass before the flow again looks like frame 12. Otherwise the flow continues unchanged for months. A 16 mm colour movie of the Hele-Shaw flow is available.

4. Discussion and summary

For mercury, the first transition at R_c leads to an increase in the dimensionless slope dH/dR from 1·0 to 1·30 (where H is the product of the Nusselt and Rayleigh number). This is much larger than is expected from theory (see table 2). There is also hysteresis in the heat flux near R_c. There is non-uniqueness on the way up, in Rayleigh number, and a slightly larger heat flux on the way down. Some of the known causes of hysteresis near R_c such as that due to changing mean temperature and to viscosity variation with temperature were considered. The dimensionless parameter η_1, which is proportioned to the rate of change of mean temperature, is defined by (Krishnamurti 1968*a*)

$$\eta_1 = \frac{d^2}{\kappa \Delta T} \frac{\partial T}{\partial t}.$$

When η_1 is non-zero it has been shown that a finite amplitude instability is possible, and the minimum Rayleigh number $R_{\min}$ at which flow, which is necessarily hexagonal, can occur is $R_{\min} = R_c(\eta_1) - (8{\cdot}1)\eta_1^2$, for η_1 small. In the present experiments η_1 was at most 10^{-3} so the effect could not have been measured. Similarly, a dimensionless parameter η_2, which is proportional to change of

viscosity with temperature and a third parameter η_3 proportional to the change of thermal conductivity with temperature are defined by

$$\eta_2 = \frac{\Delta T}{\nu}\frac{\partial \nu}{\partial T}, \quad \eta_3 = \frac{\Delta T}{k}\frac{\partial k}{\partial T}.$$

The minimum Rayleigh numbers at which finite amplitude instability can occur can be determined from Busse's calculations (1967). Using $\partial\nu/\partial T = 3{\cdot}5 \times 10^{-3}(°\mathrm{C})^{-1}$ and $\partial k/\partial T = 1{\cdot}5 \times 10^{-3}(°\mathrm{C})^{-1}$ for mercury, it was found that neither of these effects is large enough to explain the observations. There is also the possibility that higher transitions, which were well separated from that at R_c for high Pr, are excited near R_c for low Pr.

The second increase in slope for mercury occurs at $R = (2{\cdot}3 \pm 0{\cdot}1) \times 10^3$. This coincides within experimental error with the Rayleigh number R_t at which the flow becomes time dependent. The observed value is $R_t = (2{\cdot}4 \pm 0{\cdot}1) \times 10^3$. This is to be compared with Busse's result $R_t - R_c = 1{\cdot}94 \times 10^{-4} R_c$ for $Pr = 2{\cdot}5 \times 10^{-2}$ and two free boundaries. The observed periods at $R \gtrsim R_t$ were of order d^2/ν and not of order d^2/κ as with the high Prandtl number fluids. This new result for mercury shows that the periods of oscillation are in fact not independent of Prandtl number, and is reflected in the discrepancy with Busse's (1972) equation (5.2), which is independent of Prandtl number. Thus the observed periods at the observed R_t would correspond to wavelengths of 200 times the depth, which is many times the lateral dimensions of the tank. Busse has expanded the stationary two-dimensional fields and the Rayleigh number in powers of $A\,Pr$, where A is the amplitude. The disturbance fields and their growth rate are expanded in powers of the wavenumber b. In obtaining Busse's equation (5.1), the Prandtl-number dependence is retained to order Pr^2 by means of the last relation of his equation (2.7) relating R to A and Pr. However, the solubility conditions and the critical amplitude A_i for instability are obtained for $Pr = 0$. For $Pr = 0$ and $A = A_i$, the most unstable mode has wavenumber $b = 0$. However, for $A > A_i$, modes with $b \neq 0$ have maximum growth rate. The period τ (Busse's equation (5.2)), which is related inversely to the imaginary part of the growth rate, is determined to first order in b. All the results are for two free boundaries, so that quantitative agreement should not be expected. It should be pointed out, however, that for air, $Pr = 0{\cdot}71$, Busse's equation (5.2) gives excellent agreement with observations. Using the observed R_t and the observed periods, the wavelength of the oscillation is 1·2 in units of the layer depth, in reasonable agreement with the observations of Willis & Deardorff (1970).

The third change of slope for mercury occurs at $R = (3{\cdot}3 \pm 0{\cdot}1) \times 10^3$, while it is seen from figure 3 that many higher frequencies are excited at

$$R \geqslant (3{\cdot}15 \pm 0{\cdot}05) \times 10^3.$$

The higher heat-flux transitions for mercury show no hysteresis upon decrease of R, but the data lie on curves rather than on straight-line segments. When comparing figure 1 with figure 3 of II, which shows straight-line segments for R increased from below and curves of larger heater flux for R decreased from above, one possible explanation is that the mercury layer is excited to the higher

heat-flux curve by finite amplitude instability on the way up. The decreasing slope at the upper limits of the data (figure 1) appear to be related to this point also. The presence of hysteresis can imply a finite amplitude instability, but the converse cannot be implied from a lack of hysteresis.

The following summary may be made of the transition studies for air, $Pr = 0{\cdot}71$. In steady-state experiments with aluminum boundaries an increase in slope at $R = R_c = 1{\cdot}7 \times 10^3$ and an increase in slope at $R = R_t = (5{\cdot}6 \pm 0{\cdot}1) \times 10^3$ are observed. The latter coincides with the onset of time dependence. No change in slope at $8{\cdot}2 \times 10^3$ is observed but a decrease in slope at $R \simeq 1{\cdot}0 \times 10^4$ and a decrease in slope at $R \simeq 1{\cdot}7 \times 10^4$ are seen. This may be related to finite amplitude instability and excitation of higher heat-flux curves. In quasi-steady experiments with aluminum boundaries (Willis & Deardorff 1967*b*) an increase in slope at $R = R_c$ and an increase in slope at $8{\cdot}2 \times 10^3$ are seen. The existing data on the onset of time dependence for $Pr = 0{\cdot}71$ are in much better agreement than are the data on heat-flux slopes. In steady-state experiments with aluminum boundaries, time-dependent flow starts at $R = R_t = (5{\cdot}6 \pm 0{\cdot}1) \times 10^3$. Quasi-steady experiments give $R_t = 6{\cdot}3 \times 10^3 \pm 500$ (Willis & Deardorff 1965), $R_t = 5{\cdot}6 \times 10^3$ (Willis & Deardorff 1967*a*) and $R_t = 5{\cdot}8 \times 10^3$ (Willis & Deardorff 1970). In the latter case, flow visualization through an upper glass boundary by means of a 'smoke' of oil droplets showed transverse oscillation of rolls in addition to occasional mean flow. The experiments lasted only 15 min after introduction of smoke.

Although $k_{\text{glass}} \gg k_{\text{air}}$ the relative magnitudes of κ, which are important for time-dependent processes, are reversed: $\kappa = 5{\cdot}0 \times 10^{-3}\,\text{cm}^2/\text{s}$ for glass and $\kappa = 0{\cdot}26\,\text{cm}^2/\text{s}$ for air. For example, if a boundary has relatively low thermal diffusivity, hot rising fluid will warm up the boundary locally above the temperature of the rising region. The fluid could nevertheless transfer the heat supplied to it from below by having the rising regions change from place to place, thus not making one location too warm, but spreading the heat. The nature of the boundary can demand or determine time dependence of the flow. Yet this appears not to be the case, since the time dependence sets in for glass and for aluminum boundaries at nearly equal R_t and with comparable periods.

For R just above R_c, it has been shown that rolls tend to meet most of the lateral boundaries at right angles. When rolls are curved R_{II} is found to be lowered. This is significant since curved rolls (due to either initial or boundary conditions) are the rule rather than the exception in most experiments.

Finally the nature of the time dependence for high Prandtl number has been described. By choosing a fluid of relatively large α and small κ, growing plumes become very distinct and can be seen moving with the larger scale flow. This is especially clear in a Hele-Shaw cell. The experiments to date are summarized in the regime diagram of figure 4.

This research was supported at the Florida State University by grant GK 18136 from the National Science Foundation. Facilities of the Geophysical Fluid Dynamics Institute, which is supported by the Office of Naval Research Contract N 00014-68-A-0159, were used. I wish to acknowledge the competent work of

J. Reeves, C. Silas and C. Love in building the apparatus, and to thank them for their freely given assistance. Part of the work was done while visiting the Advanced Study Program at the National Center for Atmospheric Research. I am grateful for the hospitality extended to me. NCAR is sponsored by the National Science Foundation.

REFERENCES

BENNING, A. F. & MARKWOOD, W. H. 1939 *Refrig. Engng*, **37**, 243–47.
BUSSE, F. H. 1967 *J. Fluid Mech.* **30**, 625.
BUSSE, F. H. 1968 *J. Math. & Phys.* **46**, 140.
BUSSE, F. H. 1972 *J. Fluid Mech.* **52**, 97.
CHEN, M. M. & WHITEHEAD, J. A. 1968 *J. Fluid Mech.* **31**, 1.
DAVIS, S. H. 1967 *J. Fluid Mech.* **30**, 465.
ELDER, J. W. 1967 *J. Fluid Mech.* **27**, 609.
HELE-SHAW, H. S. J. 1898 *Trans. Inst. Nav. Arch.* **40**, 21.
KOSCHMIEDER, L. 1966 *Beit. Z. Phys. Atmos.* **39**, 1.
KRISHNAMURTI, R. 1967 Ph.D. dissertation, University of California, Los Angeles.
KRISHNAMURTI, R. 1968*a* *J. Fluid Mech.* **33**, 445.
KRISHNAMURTI, R. 1968*b* *J. Fluid Mech.* **33**, 457.
KRISHNAMURTI, R. 1970*a* *J. Fluid Mech.* **42**, 295.
KRISHNAMURTI, R. 1970*b* *J. Fluid Mech.* **42**, 309.
LAMB, H. 1932 *Hydrodynamics*. Dover.
MALKUS, W. V. R. 1954 *Proc. Roy. Soc.* A **225**, 185.
ROSSBY, H. T. 1966 Ph.D. dissertation, Massachusetts Institute of Technology.
SCHLÜTER, A., LORTZ, D. & BUSSE, F. 1965 *J. Fluid Mech.* **23**, 129.
SCHNECK, P. & VERONIS, G. 1967 *Phys. Fluids*, **10**, 924.
SEGEL, L. A. 1969 *J. Fluid Mech.* **38**, 203.
WILLIS, G. E. & DEARDORFF, J. W. 1965 *Phys. Fluids*, **8**, 2225.
WILLIS, G. E. & DEARDORFF, J. W. 1967*a* *Phys. Fluids*, **10**, 931.
WILLIS, G. E. & DEARDORFF, J. W. 1967*b* *Phys. Fluids*, **10**, 1861.
WILLIS, G. E. & DEARDORFF, J. W. 1970 *J. Fluid Mech.* **44**, 661.

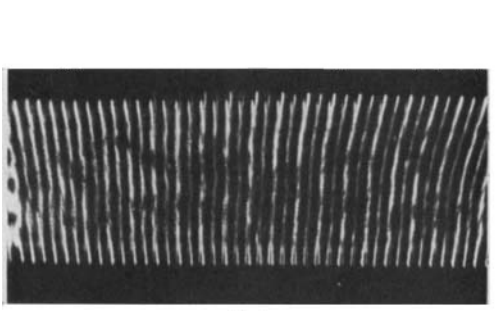

(*a*)

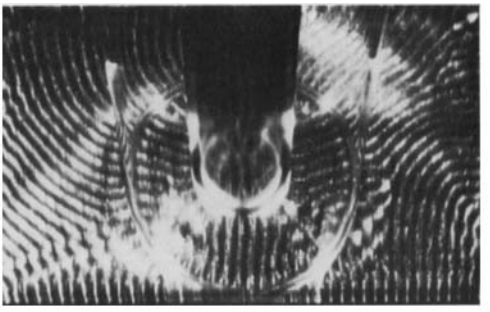

(*b*)

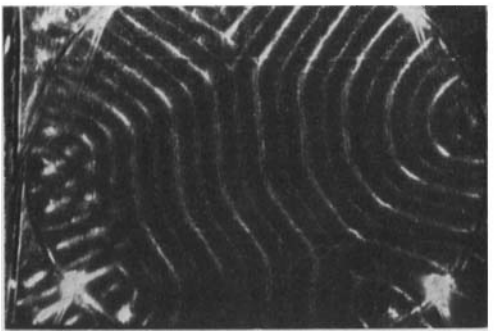

(*c*)

(*d*)

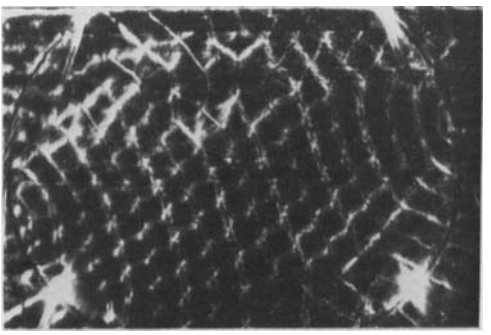

(*e*)

FIGURE 5. The preferred orientation of rolls for various side-wall geometries. $Pr = 0{\cdot}86 \times 10^3$. (*a*) Rolls parallel to the short side of a rectangular container, $R = 1{\cdot}1R_c$. (*b*) Rolls in the annular region between two circular cylinders, $R = 1{\cdot}1R_c$. (*c*) Rolls in a circular region, aspect ratio 22, $R = 1{\cdot}2R_c$. (*d*) As (*c*) but $R = 8R_c$. (*e*) As (*c*) but $R = 10R_c$.

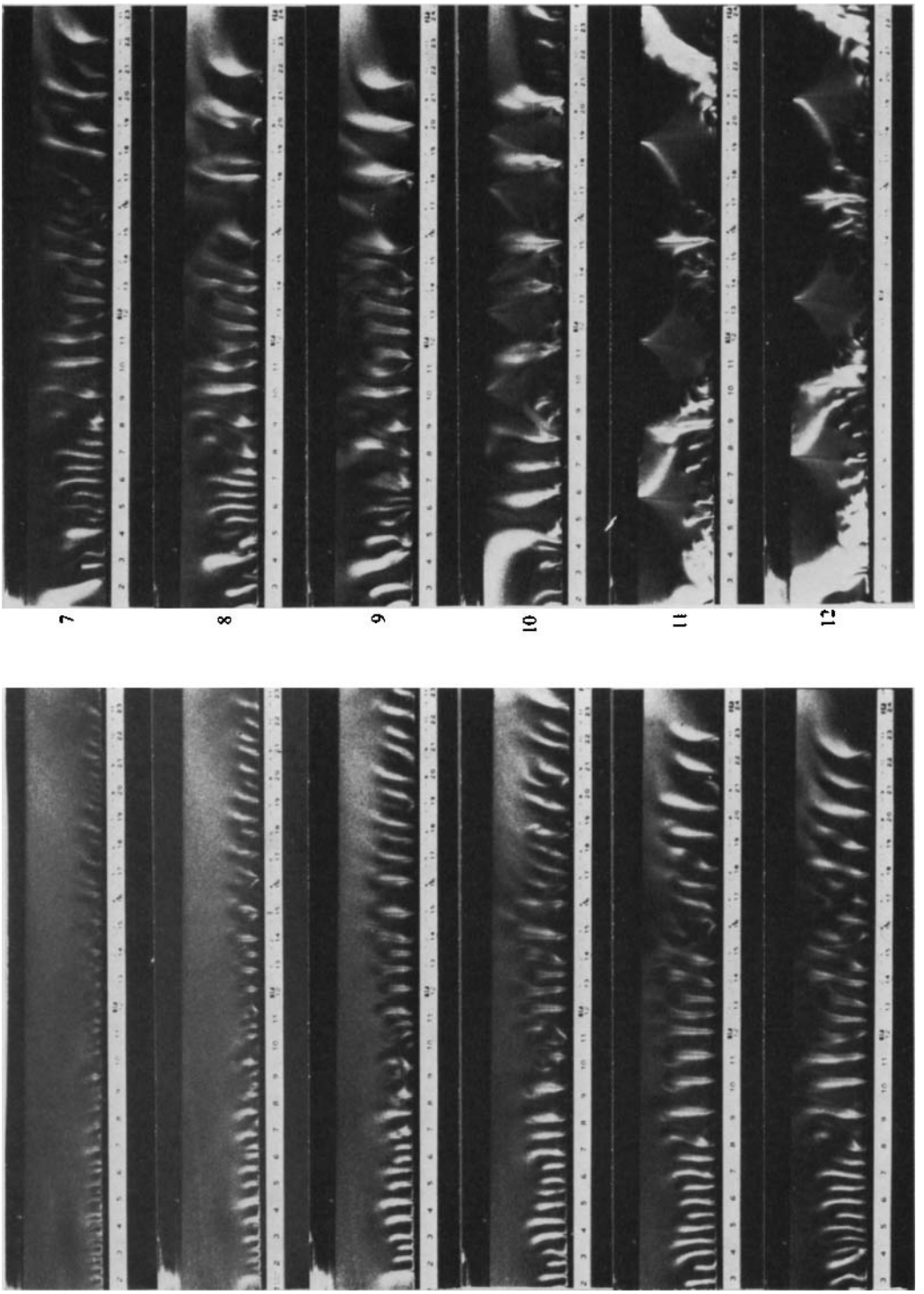

FIGURE 6. A sequence of photographs showing the growth and attainment of the final state of flow in a Hele-Shaw cell which is heated uniformly and steadily from below. The first frame was taken a few seconds after heating was started. The first three are several seconds apart, the next three are several minutes apart and the last was taken about 30 h after heating was started. The scale below each photo is in inches. $R = 2 \times 10^8 = 5{\cdot}4 \times 10^3\, R_c$.

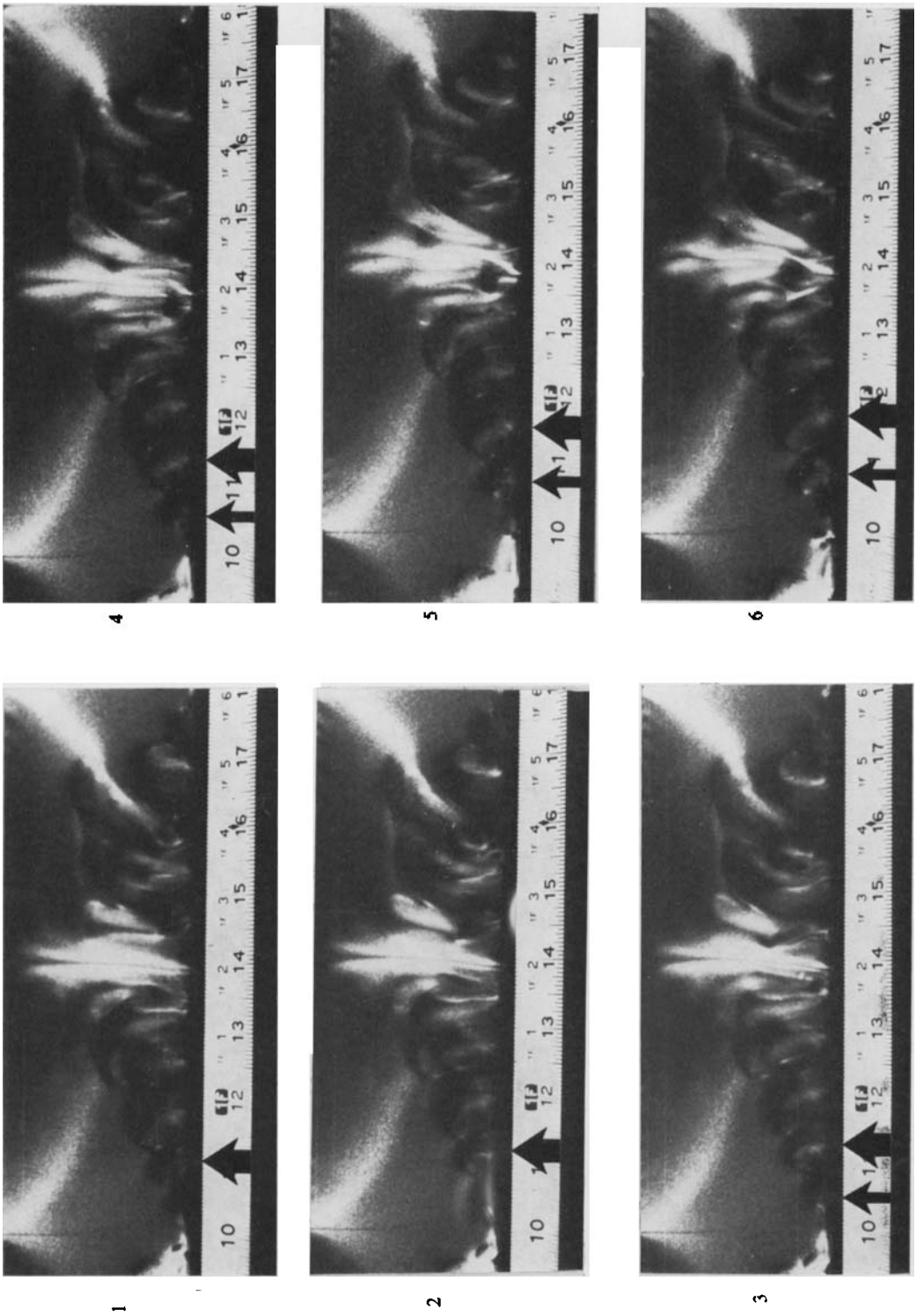

FIGURE 7(*a*). For legend see plate 4.

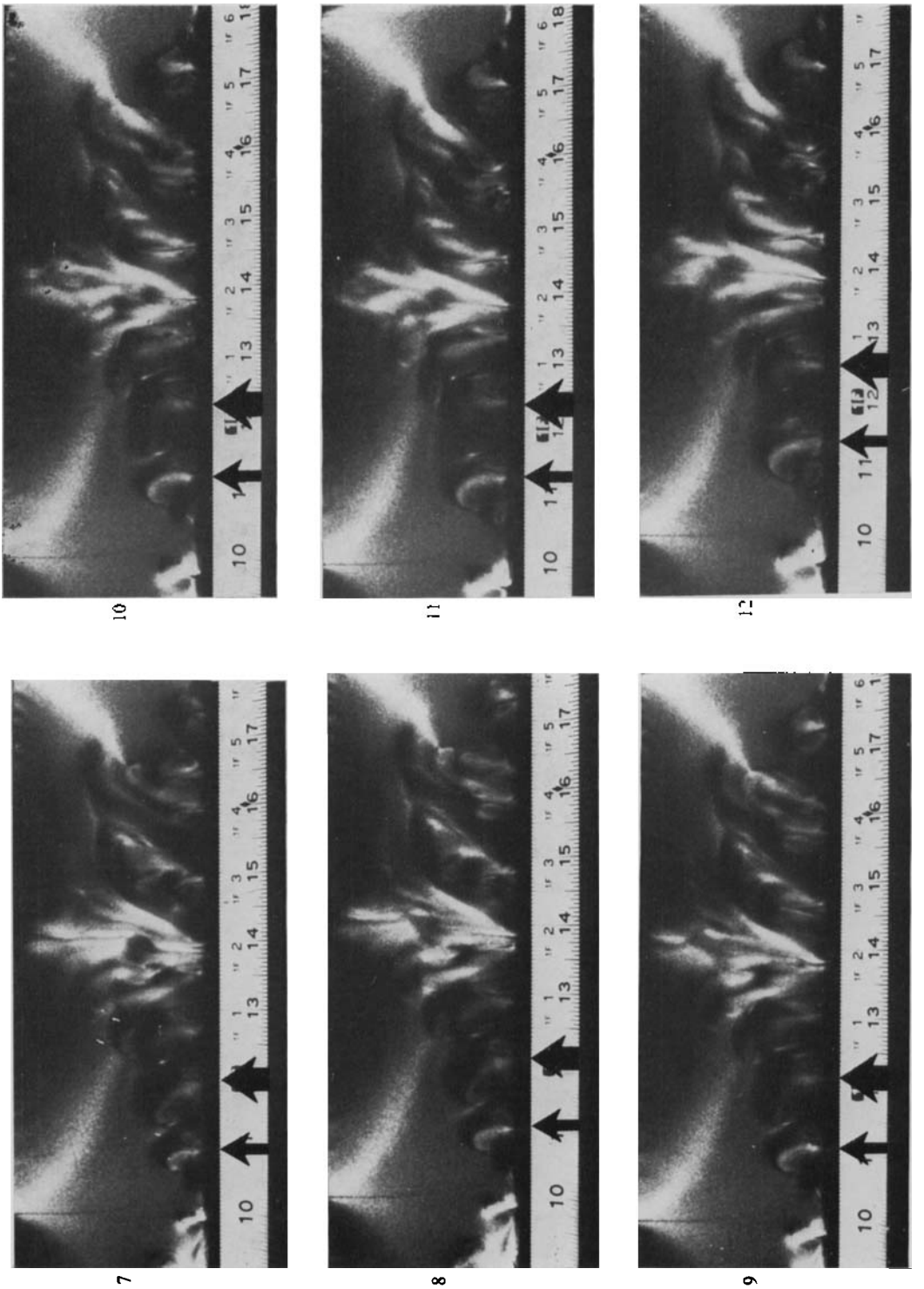

FIGURE 7(*b*). Close-up view of the time-dependent flow in a Hele-Shaw cell with steady heating. The photographs were taken at 3 s intervals. The larger arrow indicates the position of one thermal as it grows and moves to the right. The smaller arrow follows another thermal as it grows and moves. $R = 2 \times 10^8 = 5{\cdot}4 \times 10^2 R_c$.